Electronic Supplementary Material (ESI) for Physical Chemistry Chemical Physics.

Supporting Information

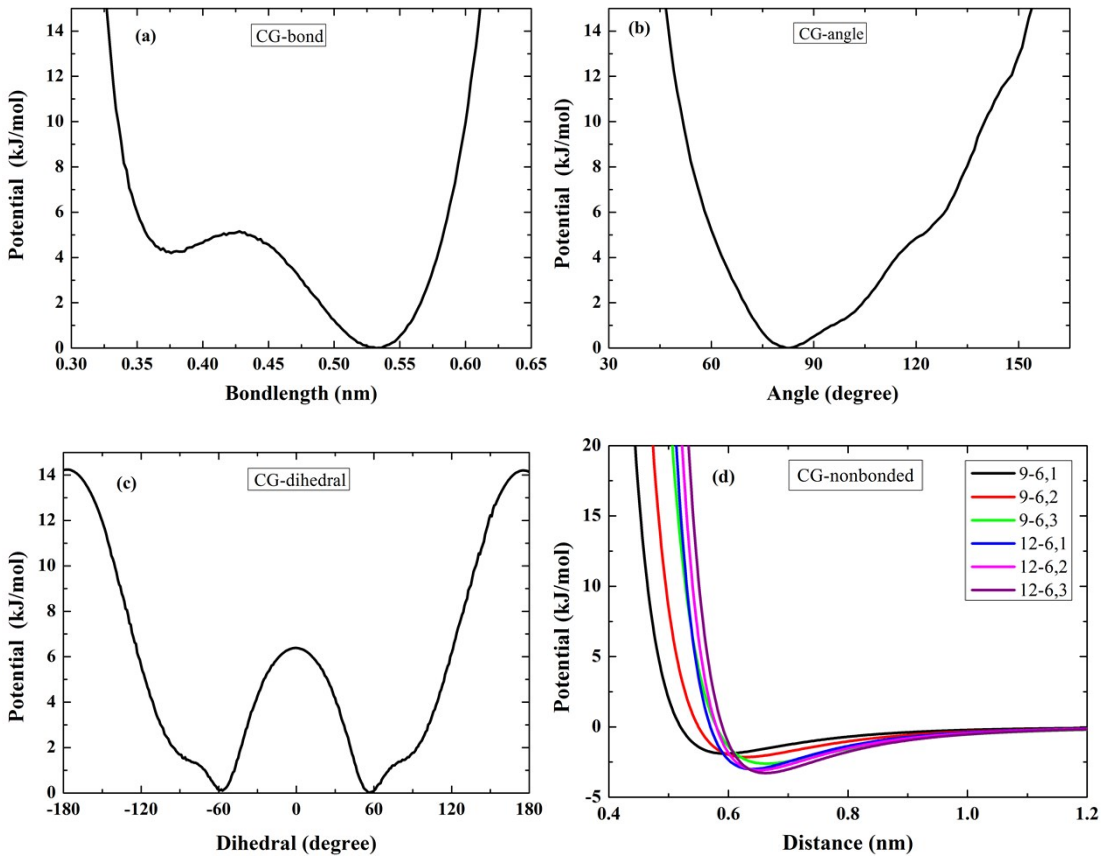

Figure S1. Interaction potentials in CG degrees of freedom for CG models: (a) bond length, (b) bending angle, (c) dihedral angle, and (d) non-bonded LJ type of potentials.

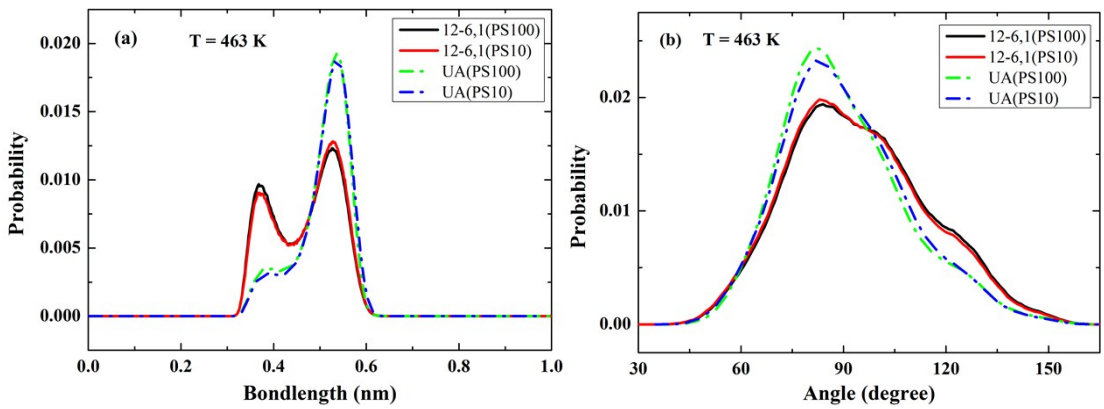

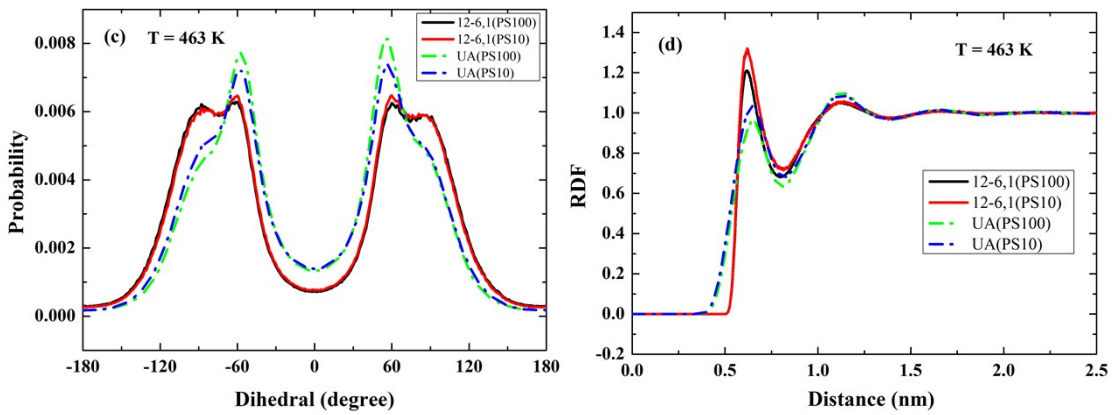

Figure S2. The probability distribution functions: (a) bond length, (b) bending angle, (c) dihedral angle, and (d) non-bonded RDF at 463 K for the PS10 and PS100 systems. CG simulations using LJ 12-6,1 potential are compared to UA counterparts.

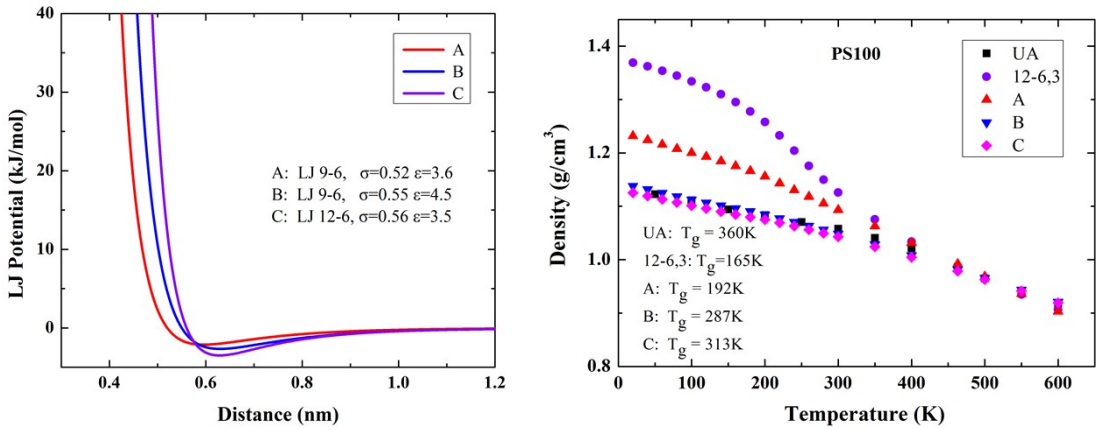

Figure S3. (a) The LJ potential in CG models with the bonded potentials derived from IBI method while the non-boned potentials still obtained by our combined method, which grows harder from A to C (left graph), and (b) the resulting bulk densities and Tg (right graph) compared with the results of UA counterpart and CG simulations with LJ 12-6,3 potential (σ = 0.59 nm, ε = 3.3 kJ/mol).

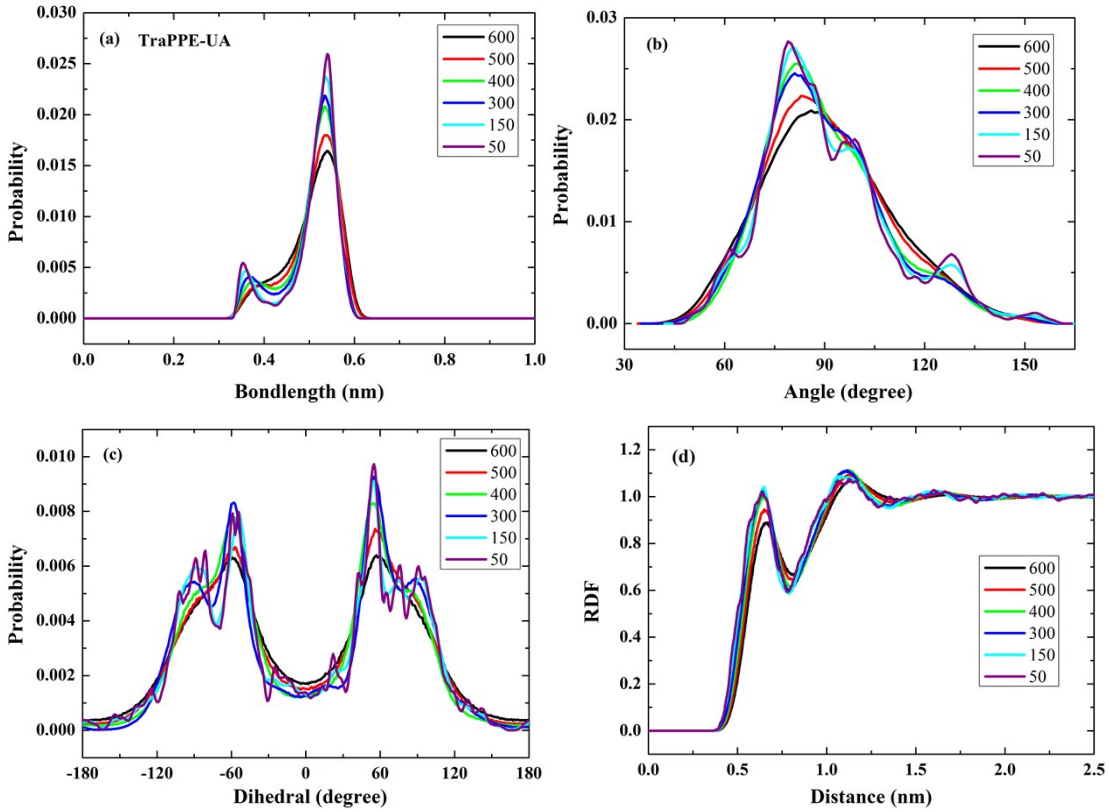

Figure S4. Temperature dependence of local conformational distributions (described in the CG degrees of freedom) in UA simulations for PS100 systems: (a) bond length, (b) bending angle, (c) dihedral angle, and (d) non-bonded RDF.

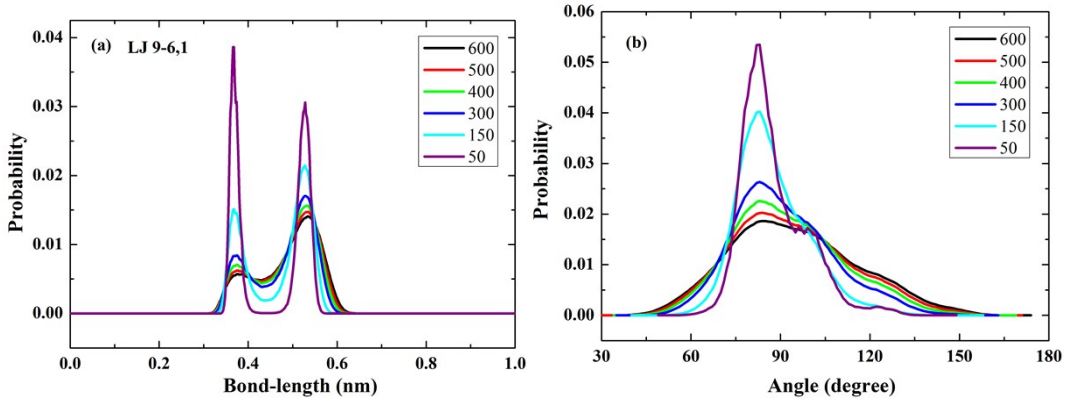

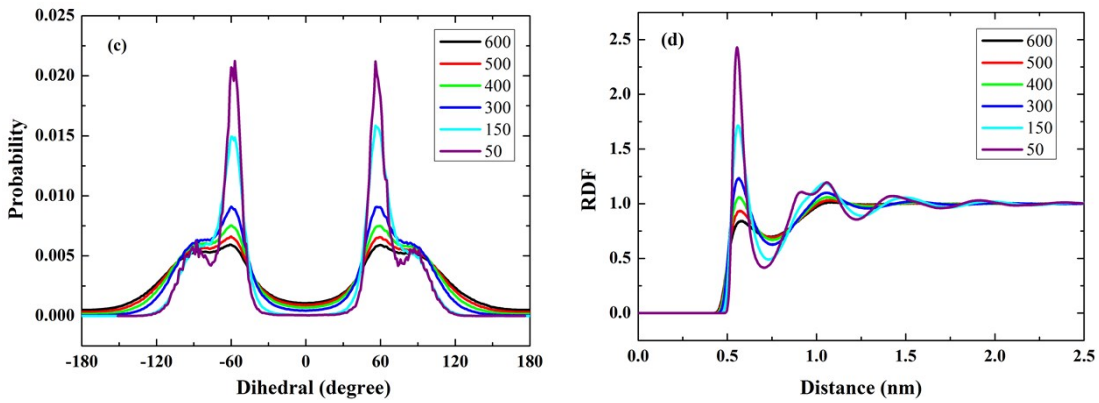

Figure S5. Temperature dependence of bonded distribution functions and non-bonded RDFs for LJ 9-6,1 potential in PS100 systems: (a) bond length, (b) bending angle, (c) dihedral angle, and (d) non-bonded RDF.

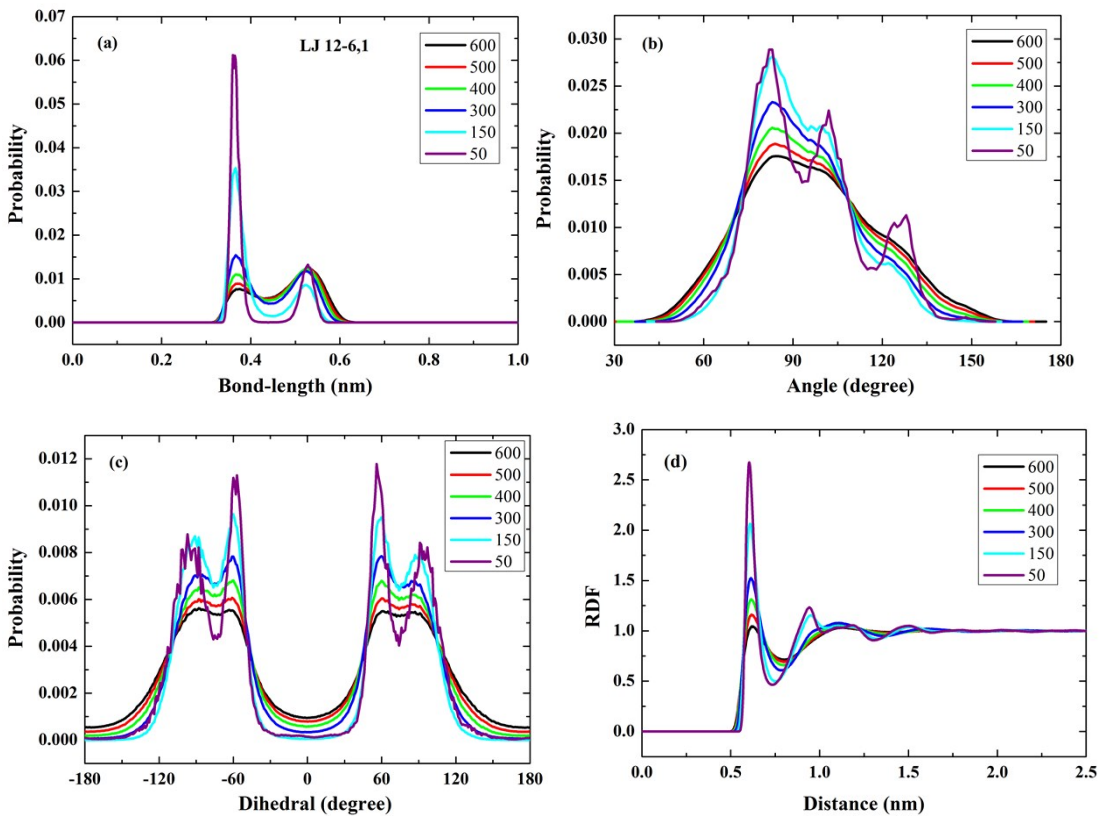

Figure S6. Temperature dependence of bonded distribution functions and non-bonded RDFs for LJ 12-6,1 potential in PS100 systems: (a) bond length, (b) bending angle, (c) dihedral angle, and (d) non-bonded RDF.

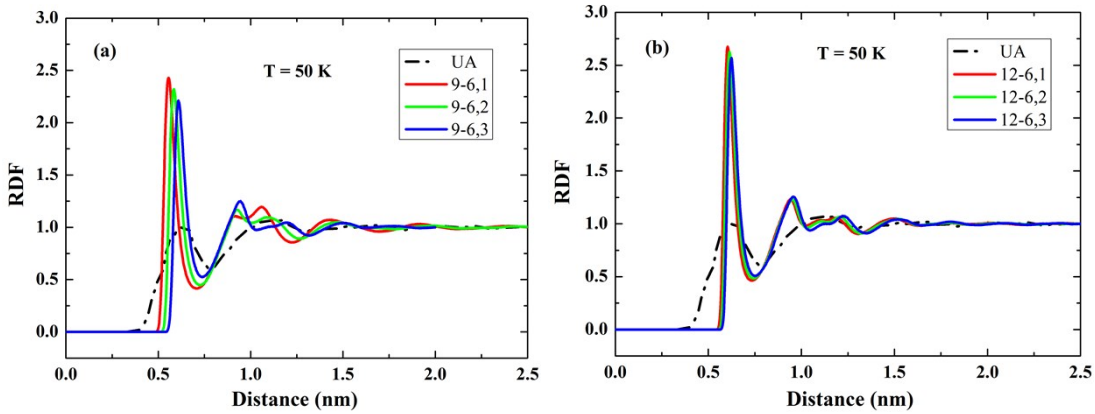

Figure S7. Non-bonded RDFs at 50 K for (a) LJ 9-6 type of potentials and (b) LJ 12-6 type of potentials, in the PS100 systems as compared with the UA results.

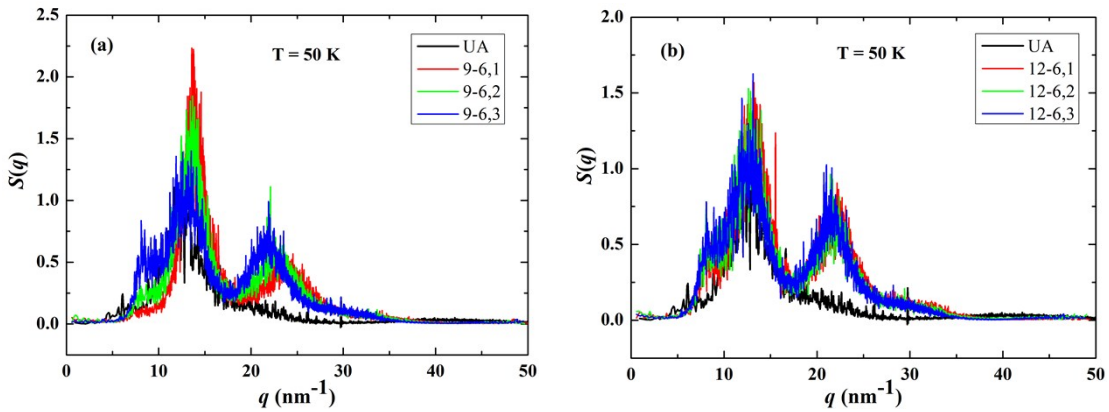

Figure S8. Calculated structure factor at 50 K for (a) LJ 9-6 type of potentials and (b) LJ 12-6 type of potentials, as compared with the UA results.

Table S1. Gyration radius R_g, components of the inertia tensor R_{11}, R_{22} and R_{33}, asphericity b, acylindricity c and relative shape anisotropy κ^2 of PS100 at 600 K.

	R_g (nm)	R_{11} (nm)	R_{22} (nm)	R_{33} (nm)	b	c	κ^2
UA	2.499± 0.001	1.613± 0.001	1.425± 0.001	1.266± 0.001	0.787± 0.002	0.429± 0.002	0.022± 0.001
9-6,1	2.364± 0.001	1.452± 0.001	1.363± 0.001	1.272± 0.001	0.370± 0.002	0.240± 0.002	0.007± 0.001
9-6,2	2.399± 0.001	1.480± 0.001	1.381± 0.001	1.287± 0.001	0.408± 0.002	0.252± 0.002	0.007± 0.001
9-6,3	2.391± 0.001	1.462± 0.001	1.376± 0.001	1.297± 0.001	0.348± 0.001	0.210± 0.002	0.005± 0.001
12-6,1	2.419±	1.494±	1.388±	1.300±	0.424±	0.238±	0.007±

	0.001	0.001	0.001	0.001	0.001	0.001	0.001
12-6,2	2.401± 0.001	1.476± 0.001	1.388± 0.001	1.287± 0.001	0.388± 0.001	0.270± 0.001	0.007± 0.001
12-6,3	2.403± 0.001	1.476± 0.001	1.385± 0.001	1.294± 0.001	0.382± 0.001	0.243± 0.001	0.007± 0.001

Table S2. Gyration radius R_g, components of the inertia tensor R_{11}, R_{22} and R_{33}, asphericity b, acylindricity c and relative shape anisotropy κ^2 of PS100 at 300 K.

	R_g (nm)	R_{11} (nm)	R_{22} (nm)	R_{33} (nm)	b	c	κ^2
UA	2.463± 0.001	1.610± 0.001	1.397± 0.001	1.233± 0.001	0.858± 0.002	0.432± 0.002	0.024± 0.001
9-6,1	2.269± 0.001	1.402± 0.001	1.303± 0.001	1.218± 0.001	0.375± 0.002	0.216± 0.002	0.007± 0.001
9-6,2	2.334± 0.001	1.481± 0.001	1.317± 0.001	1.231± 0.001	0.569± 0.002	0.221± 0.002	0.013± 0.001
9-6,3	2.249± 0.001	1.434± 0.001	1.359± 0.001	1.269± 0.001	0.330± 0.001	0.235± 0.002	0.005± 0.001
12-6,1	2.314± 0.001	1.429± 0.001	1.333± 0.001	1.238± 0.001	0.387± 0.001	0.247± 0.001	0.007± 0.001
12-6,2	2.304± 0.001	1.425± 0.001	1.333± 0.001	1.225± 0.001	0.394± 0.001	0.276± 0.001	0.008± 0.001
12-6,3	2.289± 0.001	1.420± 0.001	1.312± 0.001	1.226± 0.001	0.405± 0.001	0.218± 0.001	0.008± 0.001

Table S3. Gyration radius R_g, components of the inertia tensor R_{11}, R_{22} and R_{33}, asphericity b, acylindricity c and relative shape anisotropy κ^2 of PS100 at 50 K.

	R_g (nm)	R_{11} (nm)	R_{22} (nm)	R_{33} (nm)	b	c	κ^2
UA	2.198± 0.001	1.457± 0.001	1.281± 0.001	1.035± 0.001	0.766± 0.002	0.569± 0.002	0.036± 0.001
9-6,1	1.973± 0.001	1.204± 0.001	1.117± 0.001	1.093± 0.001	0.229± 0.002	0.054± 0.002	0.004± 0.001
9-6,2	2.255± 0.001	1.343± 0.001	1.311± 0.001	1.250± 0.001	0.164± 0.002	0.156± 0.002	0.002± 0.001
9-6,3	2.135± 0.001	1.275± 0.001	1.254± 0.001	1.166± 0.001	0.159± 0.001	0.213± 0.002	0.003± 0.001
12-6,1	2.136± 0.001	1.336± 0.001	1.198± 0.001	1.159± 0.001	0.395± 0.001	0.093± 0.001	0.008± 0.001

12-6,2	2.142± 0.001	1.326± 0.001	1.207± 0.001	1.171± 0.001	0.345± 0.001	0.086± 0.001	0.006± 0.001
12-6,3	2.161± 0.001	1.363± 0.001	1.310± 0.001	1.046± 0.001	0.621± 0.001	0.452± 0.001	0.023± 0.001

Table S4. Diffusion coefficient *D* and scaling factor *f* for different LJ potentials obtained from CG simulations at 463K.

	9-6,1	9-6,2	9-6,3	12-6,1	12-6,2	12-6,3
D(PS10), 10^{-6}cm^2/s	20.9±0.1	15.4±0.1	7.8±0.1	7.4±0.1	7.2±0.1	5.7±0.1
f (PS10)	20.7	15.3	7.7	7.3	7.1	5.7
D(PS100), 10^{-7}cm^2/s	12.4±0.1	6.0±0.1	4.0±0.1	3.4±0.1	3.1±0.1	2.3±0.1
f (PS100)	134.8	65.2	43.5	37.0	33.7	25.0